Electronic Supplementary Material (ESI) for Chemical Science.
This journal is © The Royal Society of Chemistry 2020

# Supporting Information I: Supplemental Experimental Data

## Redox Mediators Accelerate Electrochemically-Driven Solubility Cycling of Molecular Transition Metal Complexes

Katherine J. Lee,[a,†] Kunal M. Lodaya,[a,†] Cole T. Gruninger,[a] Eric S. Rountree,[†] and Jillian L. Dempsey[†]

[†] Department of Chemistry, University of North Carolina at Chapel Hill, Chapel Hill, North Carolina, USA 27599

[a.] These authors contributed equally.

*Table of Contents* *Page*

## General Experimental Details

**General Considerations**. All chemical syntheses were performed using either a nitrogen-filled glovebox or a high-vacuum manifold with standard Schlenk techniques. Solvents were degassed with argon and dried using a solvent system (Pure Process Technology). Water for polishing was obtained from a Milli-Q system. Tetrabutylammonium hexafluorophosphate (TCI, > 98%) was recrystallized from hot ethanol, washed with cold ethanol, and dried under vacuum for 8 hours at 80ºC. $[Ni(P^{Ph}{}_2N^{Ph}{}_2)_2(CH_3CN)][BF_4]$ was synthesized and recrystallized according to literature methods and characterized via NMR.[13] NMR spectra were recorded on a Bruker 600 MHz spectrometer.

**Electrochemical Methods**. All electrochemical measurements were performed in a nitrogen-filled glovebox using electrode leads that were fed through a custom port and connected to a WaveDriver potentiostat (Pine Research Instrumentation). Measurements were performed using a standard three-electrode configuration with a glassy carbon working electrode (CH Instruments, 3 mm diameter), platinum wire counter electrode, and silver wire pseudoreference electrode immersed in glass tubes filled with 0.25 M $[NBu_4][PF_6]$ acetonitrile and isolated from the main cell compartment via a porous Vycor frit. Glassy carbon working electrodes were polished using a Milli-Q water slurry of 0.05 $\mu$m polishing powder (CH Instruments, no agglomerating agents), rinsed and sonicated in Milli-Q water, and rinsed with acetone. Working electrodes were electrochemically pretreated with three cyclic scans between 0.7 V to -2.8 V vs $Fc^{+/0}$ couple (approximately) at 0.1 V $s^{-1}$ in 0.25 M $[NBu_4][PF_6]$ acetonitrile solution.

**Spectroelectrochemistry Methods.** Thin layer UV-vis spectroelectrochemistry obtained in a nitrogen-filled glovebox using an OceanOptics DH-mini light source fiber coupled to an OceanOptics Flame spectrometer and a WaveDriver potentiostat (Pine Research Instrumentation). Measurements performed in Honeycomb Spectroelectrochemical Cell Kit (Pine Research Instrumentation, model: AKSTCKIT3) using a Platinum Honeycomb Electrode (Pine Research Instrumentation, model: AB01STC1PT) and a silver wire pseudo-reference.

## SI-1 Cyclic voltammetry of $[Ni(P^{Ph}{}_2N^{Ph}{}_2)_2]^{2+}$

### *Variable scan rate cyclic voltammograms*

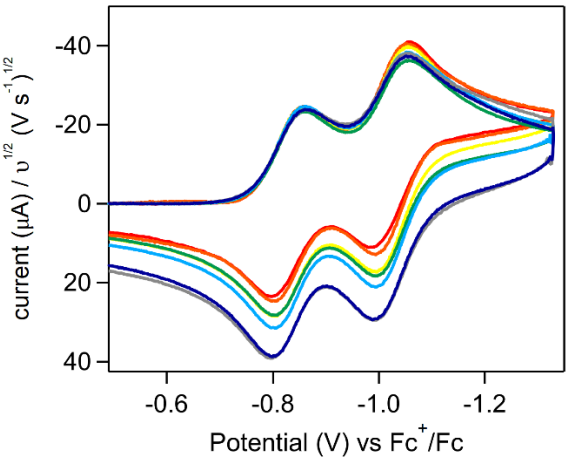


**Figure S1** Cyclic voltammograms of 0.5 mM $[Ni(P^{Ph}{}_2N^{Ph}{}_2)_2]^{2+}$ recorded at 0.025 (red), 0.05 (orange), 0.1 (yellow), 0.5 (green), 1 (light blue), 5 (blue), and 10 (grey) V $s^{-1}$. Voltammograms obtained in 0.25 M $[NBu_4][PF_6]$ acetonitrile using a glassy carbon working electrode and normalized by $\upsilon^{1/2}$.

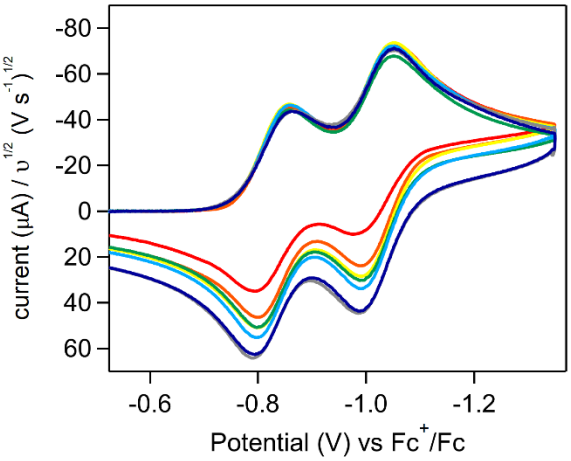


**Figure S2** Cyclic voltammograms of 1 mM $[Ni(P^{Ph}{}_2N^{Ph}{}_2)_2]^{2+}$ recorded at 0.025 (red), 0.05 (orange), 0.1 (yellow), 0.5 (green), 1 (light blue), 5 (blue), and 10 (grey) V $s^{-1}$. Voltammograms obtained in 0.25 M $[NBu_4][PF_6]$ acetonitrile using a glassy carbon working electrode and normalized by $\upsilon^{1/2}$.

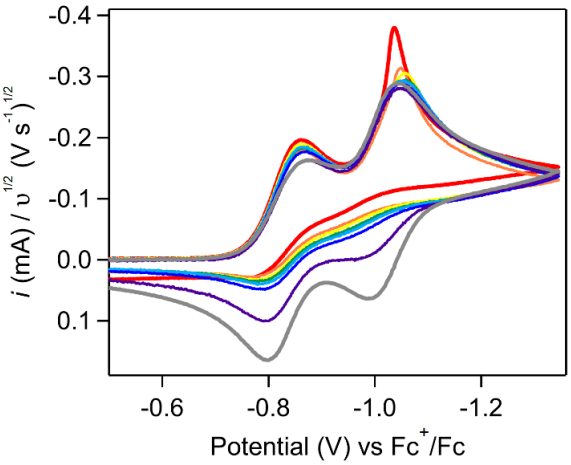


**Figure S3** Cyclic voltammograms of 4 mM $[Ni(P^{Ph}{}_2N^{Ph}{}_2)_2]^{2+}$ recorded at 0.025 (red), 0.05 (orange), 0.1 (yellow), 0.2 (green), 0.5 (light blue), 1 (dark blue), 5 (purple), and 10 (grey) V $s^{-1}$. Voltammograms obtained in 0.25 M $[NBu_4][PF_6]$ acetonitrile using a glassy carbon working electrode and normalized by $\upsilon^{1/2}$.

### *Cathodic peak currents as a function of scan rate*

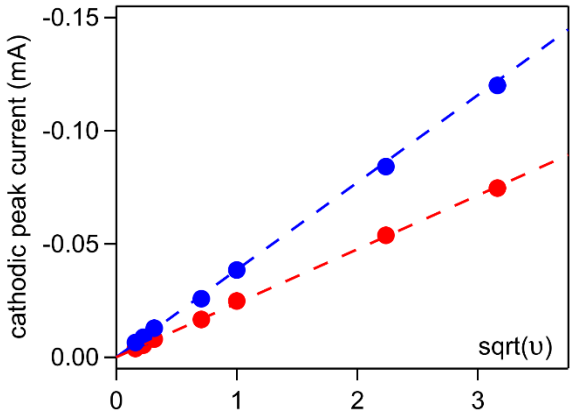


**Figure S4** Cathodic peak current as a function of $\upsilon^{1/2}$ for voltammograms collected in 0.5 mM $[Ni(P^{Ph}_2N^{Ph}_2)_2]^{2+}$ for the $Ni^{II/I}$ (red) and $Ni^{I/0}$ (blue) redox couple. Dots represent experimental data points and dashed lines represent linear fits. Linear fit for $Ni^{II/I}$ redox couple: slope = -2.38e-5 A $(V\ s^{-1})^{-1/2}$, $R^2$ = 0.99. Linear fit for the $Ni^{I/0}$ redox couple: slope = -3.86e-5 A $(V\ s^{-1})^{-1/2}$, $R^2$ = 0.99.

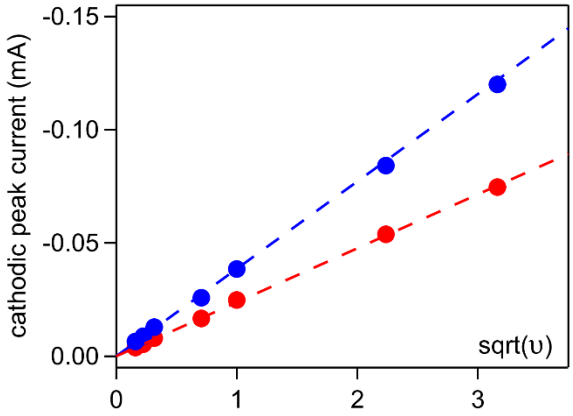


**Figure S5** 1 Cathodic peak current as a function of $\upsilon^{1/2}$ for voltammograms collected in 1 mM $[Ni(P^{Ph}_2N^{Ph}_2)_2]^{2+}$ for the $Ni^{II/I}$ (red) and $Ni^{I/0}$ (blue) redox couple. Dots represent experimental data points and dashed lines represent linear fits. Linear fit for $Ni^{II/I}$ redox couple: slope = -4.40e-5 A $(V\ s^{-1})^{-1/2}$, $R^2$ = 0.98. Linear fit for the $Ni^{I/0}$ redox couple: slope = -7.06e-5 A $(V\ s^{-1})^{-1/2}$, $R^2$ = 0.99.

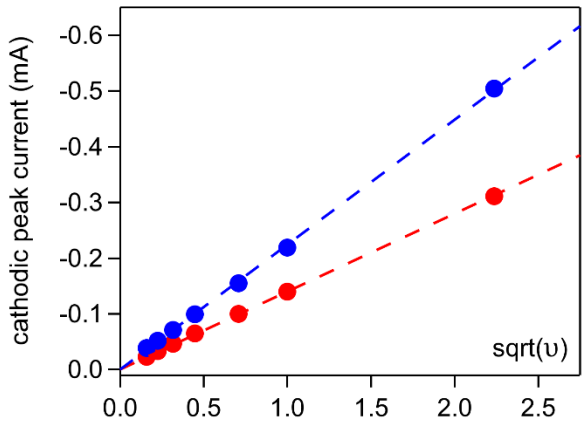


**Figure S6** Cathodic peak current as a function of $\upsilon^{1/2}$ for voltammograms collected in 3 mM $[Ni(P^{Ph}{}_2N^{Ph}{}_2)_2]^{2+}$ for the $Ni^{II/I}$ (red) and $Ni^{I/0}$ (blue) redox couple. Dots represent experimental data points and dashed lines represent linear fits. Linear fit for $Ni^{II/I}$ redox couple: slope = -1.40e-4 A $(V\ s^{-1})^{-1/2}$, $R^2$ = 0.97. Linear fit for the $Ni^{I/0}$ redox couple: slope = -2.24e-4 A $(V\ s^{-1})^{-1/2}$, $R^2$ = 0.99. Corresponding cyclic voltammograms found in main text, Figure 1B.

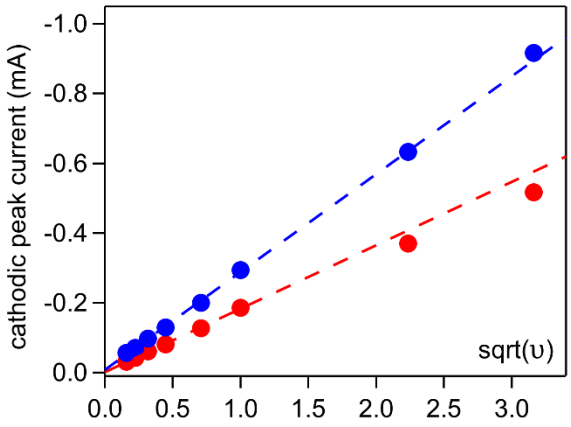


**Figure S7** Cathodic peak current as a function of $\upsilon^{1/2}$ for voltammograms collected in 4 mM $[Ni(P^{Ph}{}_2N^{Ph}{}_2)_2]^{2+}$ for the $Ni^{II/I}$ (red) and $Ni^{I/0}$ (blue) redox couple. Dots represent experimental data points and dashed lines represent linear fits. Linear fit for $Ni^{II/I}$ redox couple: slope = -1.82e-4 A $(V\ s^{-1})^{-1/2}$, $R^2$ = 0.99. Linear fit for the $Ni^{I/0}$ redox couple: slope = -2.80e-4 A $(V\ s^{-1})^{-1/2}$, $R^2$ = 0.99.

### *Diffusion coefficient of $[Ni(P^{Ph}_2N^{Ph}_2)_2]^{2+}$*

The peak current for a reversible, diffusion controlled redox process will vary linearly with $\upsilon^{1/2}$.[1] This relationship between peak current and scan rate is described by the Randles-Sevcik equation:

$$i_p = 0.4463nFAC^* \left(\frac{nF\upsilon D}{RT}\right)^{1/2} \quad \text{(S1)}$$

where $i_p$ is the peak current (A), n is the number of electrons transferred in the redox event, F is the Faraday constant, A is the electrode surface area ($cm^2$), C* is the bulk concentration of the analyte (mol $cm^{-3}$), $\upsilon$ is scan rate (V $s^{-1}$), D is the diffusion coefficient ($cm^2$ $s^{-1}$), R is the universal gas constant, and T is temperature. This relationship allows the diffusion coefficient of a homogeneous species to be determined by plotting the baseline-corrected peak current as a function of $\upsilon^{1/2}$. The linear fit of this data will yield a slope which corresponds to $0.4463nFAC^* \left(\frac{nFD}{RT}\right)^{1/2}$.

Using these equations, a diffusion coefficient for $[Ni(P^{Ph}_2N^{Ph}_2)_2]^{2+}$ was calculated from plots of the cathodic peak current of the $Ni^{II/I}$ redox couple and $\upsilon^{1/2}$. This analysis was performed using variable scan rate cyclic voltammograms collected at 0.5, 1, 3, and 4 mM $[Ni(P^{Ph}_2N^{Ph}_2)]^{2+}$.

**Table S1** Summary of linear fits for the cathodic peak current of the $Ni^{II/I}$ couple and $\upsilon^{1/2}$ and calculated diffusion coefficients as determined by the Randles-Sevick equation

| concentration (mM) | Slope (A [V $s^{-1}$]$^{1/2}$) | $R^2$ | *D* ($cm^2$ $s^{-1}$) |
|---|---|---|---|
| 0.5 | -2.38e-05 | 0.99 | 6.29e-06 |
| 1 | -4.42e-05 | 0.98 | 5.41e-06 |
| 3 | -1.40e-04 | 0.97 | 6.02e-06 |
| 4 | -1.84e-04 | 0.99 | 5.74e-06 |

The anticipated linear relationship between these slopes and the concentration of $[Ni(P^{Ph}_2N^{Ph}_2)]^{2+}$ with a slope of 0.046117 (A [V $s^{-1}$]$^{-1/2}$ $M^{-1}$) was observed. This slope – corresponding to

$0.4463nFA\left(\frac{nFD}{RT}\right)^{1/2}$ – was used to extract an average diffusion coefficient from all data sets of 5.90e-06 $cm^2s^{-1}$.

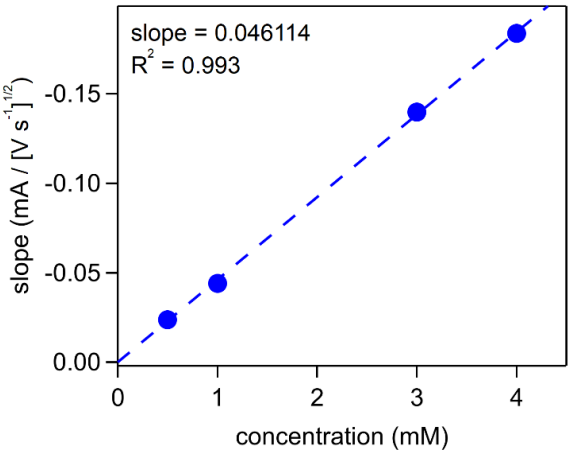


**Figure S8** A diffusion coefficient for $[Ni(P^{Ph}{}_2N^{Ph}{}_2)_2]^{2+}$ was derived based on the scan rate dependence trials by plotting the slope derived from the linear fit of the cathodic peak current for the $Ni^{II/I}$ as a function of concentration. These slopes linearly depended on concentration and the slope of this line was used to extract an average diffusion coefficient of 5.90e-06 $cm^2\ s^{-1}$.

### *Concentration dependence voltammetry*

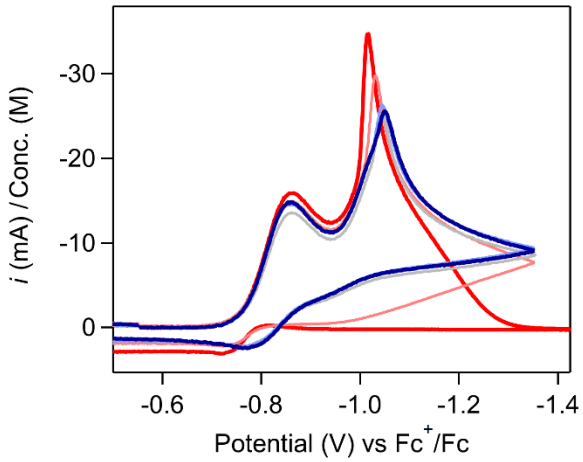


**Figure S9** Concentration dependence studies for $[Ni(P^{Ph}{}_2N^{Ph}{}_2)_2]^{2+}$. Cyclic voltammograms recorded in a solutions of 5 (blue), 5.7 (light blue), 6.7 (grey), 8 (light red), and 8.9 (red) mM $[Ni(P^{Ph}{}_2N^{Ph}{}_2)_2]^{2+}$. Voltammograms obtained in 0.25 M $[NBu_4][PF_6]$ acetonitrile at 0.1 V $s^{-1}$ using a glassy carbon working electrode and normalized to concentration of $[Ni(P^{Ph}{}_2N^{Ph}{}_2)_2]^{2+}$.

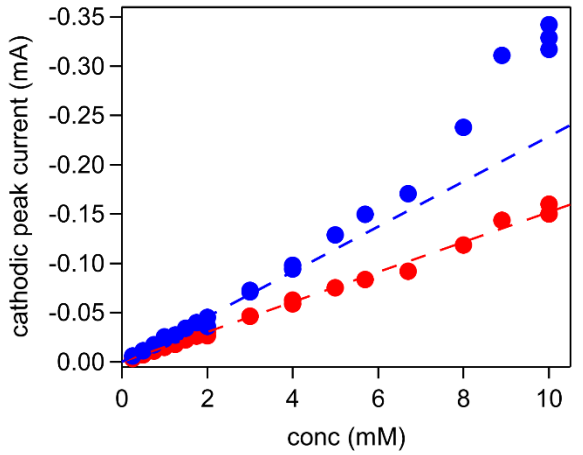


**Figure S10** Cathodic peak current for the $Ni^{II/I}$ (red) and $Ni^{I/0}$ (blue) features as a function of $[Ni(P^{Ph}{}_2N^{Ph}{}_2)_2]^{2+}$ concentration (0.25 mM – 10 mM). Dots represent experimental data and dashed lines are linear fits. Linear fit for the $Ni^{II/I}$ couple (slope = -0.015306 A $M^{-1}$, $R^2$ = 0.98) includes experimental data points for all concentrations. Linear fit for the $Ni^{I/0}$ couple (slope = -0.0229 A $M^{-1}$, $R^2$ = 0.95) only includes experimental data points for $[Ni(P^{Ph}{}_2N^{Ph}{}_2)_2]^{2+}$] concentrations up to 3 mM.

## SI-2 Additional evidence of film formation

### *Visual inspection of working electrodes*

**Figure S11** Picture of glassy carbon working electrode before **(left)** and after **(right)** chronoamperometry in 3 mM $[Ni(P^{Ph}{}_2N^{Ph}{}_2)_2]^{2+}$. Visible electrode fouling can be observed in the form of an orange film after electrochemical trials. During chronoamperometry experiments, the working electrode was held at -1.45 V for 10 min, rinsed with a minimal amount of acetonitrile, and dried under $N_2$. Picture of post-chronoamperometry working electrode is taken through the plexiglass window of the $N_2$-filled glovebox in which the electrochemical trials were conducted. Chronoamperometry conducted in 0.25 M $[NBu_4][PF_6]$ acetonitrile.

### *Additional multiple cycling experiments*

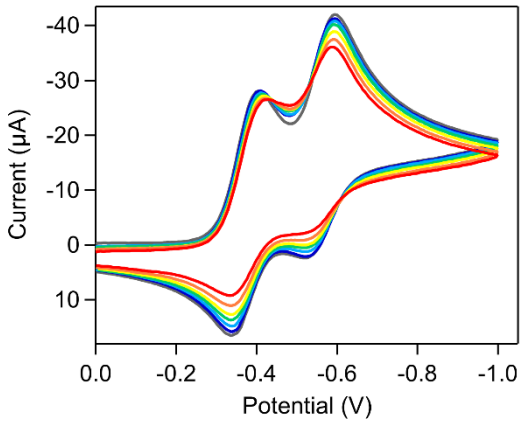


**Figure S12** Repetitive cycling experiments confirm that the electrode properties can be modified over the course of a single electrochemical measurement. Electrodes were polished and pretreat at the start of each data set and all subsequent voltammograms were collected using the same electrode without polishing between scans. The solution was stirred between scans to refresh the diffusion layer. **(A)** Rapid changes can be observed in each subsequent voltammograms collected at 10 mM $[Ni(P^{Ph}{}_2N^{Ph}{}_2)_2]^{2+}$: scan 1 (grey), 2 (dark blue), 3 (light blue), 4 (green), 5 (yellow), 6 (orange), and 7 (red). **(B)** At lower concentrations (1.75 mM $[Ni(P^{Ph}{}_2N^{Ph}{}_2)_2]^{2+}$), variability across voltammograms is more subtle and requires a larger number of scans to become observable: scan 1 (grey), 5 (dark blue), 10 (light blue), 15 (green), 20 (yellow), 25 (orange), and 30 (red). All voltammograms recorded in 0.25 M $[NBu_4][PF_6]$ acetonitrile at 0.1 V $s^{-1}$ using a glassy carbon working electrode.

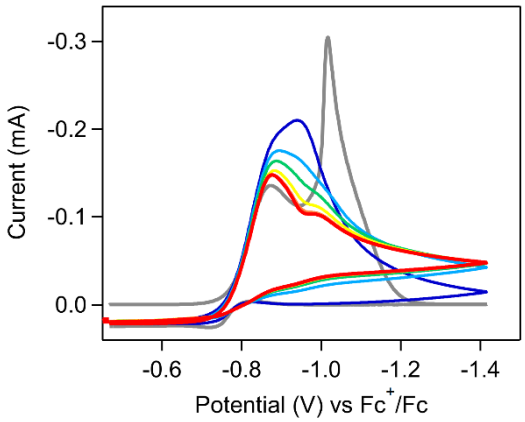


**Figure S13** Additional repetitive cycling experiments highlighting irreproducibility between experiments. Electrodes were polished and pretreated at the start of each data set and all subsequent voltammograms were collected using the same electrode without polishing between scans. The solution was stirred between scans to refresh the diffusion layer. Rapid changes can be observed in each subsequent voltammograms collected at 10 mM $[Ni(P^{Ph}{}_2N^{Ph}{}_2)_2]^{2+}$: scan 1 (grey), 2 (dark blue), 3 (light blue), 4 (green), 5 (yellow), 6 (orange), and 7 (red). Voltammograms recorded in 0.25 M $[NBu_4][PF_6]$ acetonitrile at 0.1 V $s^{-1}$ using a glassy carbon working electrode.

## SI-3 Evidence for metastability of the deposited material

### *Deposited material is weakly-adsorbed*

The ferrocene-catalyzed stripping reactivity was used to evaluate the stability of the deposited [Ni($P^{Ph}_2N^{Ph}_2$)$_2$]. In these experiments, the electrode-adsorbed [Ni($P^{Ph}_2N^{Ph}_2$)$_2$] was formed in 10 mM [Ni($P^{Ph}_2N^{Ph}_2$)$_2$]$^{2+}$ solution by collecting linear sweep voltammograms through the $Ni^{II/I}$ and $Ni^{I/0}$ redox couple until complete current inhibition was observed, ensuring that a similar amount of charge was passed in each case in order to minimize differences between the amount of deposited material (**Figure S14**). These electrodes were then used to collect a voltammogram in a ferrocene-electrolyte solution after either being rinsed with solvent, left to equilibrate in the ferrocene-electrolyte solution for 30 seconds, or dried in $N_2$. The electrodes that had been rinsed or left to equilibrate in solution consistently showed less current enhancement at the $Fc^{+/0}$ redox couple relative to electrodes that had been left to dry in $N_2$ (**Figure S15**). This data indicates that electrode-adsorbed [Ni($P^{Ph}_2N^{Ph}_2$)$_2$] is metastable and will desorb or re-dissolve upon rinsing or when no longer maintained under specific conditions.[3] As such, the process of rinsing or equilibration will corrode the surface deposits which, in turn, decreases the catalytic response observed in the ferrocene-only scan.

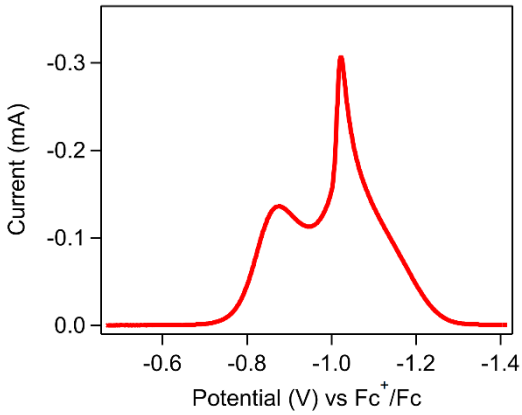


**Figure S14** Example of how the deposited material was formed. Linear sweep voltammogram collected in 10 mM [Ni($P^{Ph}_2N^{Ph}_2$)$_2$]$^{2+}$ which swept from -0.5 V to -1.4 V, ensuring that the electrode was completely passivated with heterogeneous [Ni($P^{Ph}_2N^{Ph}_2$)]. Voltammograms recorded at 0.1 V $s^{-1}$ in 0.25 M [$NBu_4$][$PF_6$] acetonitrile using a glassy carbon working electrode.

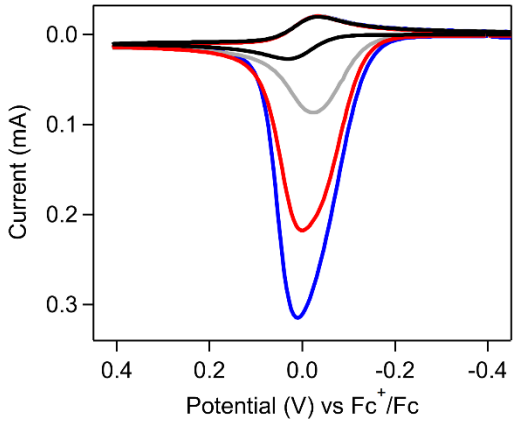


**Figure S15** Cyclic voltammogram of 2 mM ferrocene collected with a freshly polished electrode (black) or an electrode that had been fully passivated in a solution of $[Ni(P^{Ph}_2N^{Ph}_2)_2]^{2+}$ and then rinsed with acetonitrile (grey), left to equilibrate in the Fc-electrolyte solution for 30 seconds (red), or dried under $N_2$ (blue). Electrodes were passivated by collecting a linear sweep voltammogram in a 10 mM solution of $[Ni(P^{Ph}_2N^{Ph}_2)_2]^{2+}$. Voltammograms recorded at 0.1 V $s^{-1}$ in 0.25 M $[NBu_4][PF_6]$ acetonitrile using a glassy carbon working electrode.

### *Partial oxidation decreases film stability*

The "dry test" procedure described above – wherein the modified electrode is left to dry in $N_2$ before collecting a voltammogram in a Fc-electrolyte solution – was used to evaluate how partially oxidizing the material through direct electron transfer between the electrode and heterogeneous [Ni($P^{Ph}_2N^{Ph}_2$)$_2$] influences film stability. Electrodes were modified by sweeping through the $Ni^{II/I}$ and $Ni^{I/0}$ couple until complete passivation was achieved at which point either the scan was ended (**Figure S16A**, blue asterisk) or the scan direction was reversed and the potential was swept to values before (**Figure S16A**, red asterisk) or after (**Figure S16A**, grey asterisk) the broad current enhancement. Comparing subsequent scans in the Fc-only solution showed that partial oxidation of heterogeneous [Ni($P^{Ph}_2N^{Ph}_2$)$_2$] decreases the stability of the material, manifesting as a decrease in $i_{p,a}$([$Fc^{+/0}$]) (**Figure S16B**).

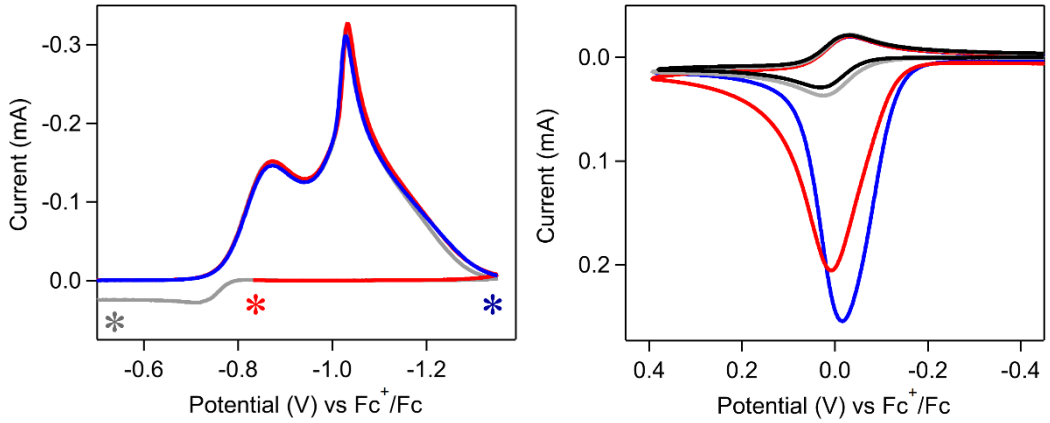


**Figure S16** Dry tests probing impact of traversing the broad current enhancement on the stability of the deposited material. **(A)** Working electrodes were modified by collecting either a linear sweep voltammogram (one segment, potential swept from -0.5 to -1.35 V, blue trace), a cyclic voltammogram with a final potential before the broad current enhancement (two segments, potential swept from -0.5 to -1.35 V and -1.35 V to -0.85 V, red trace), or a cyclic voltammogram with a final potential after the broad current enhancement (two segments, potential swept between -0.5 V to -1.35 V, grey trace). **(B)** Working electrodes were dried under $N_2$ and used to collect cyclic voltammograms in a solution of 1 mM ferrocene. Cyclic voltammogram obtained with a freshly polished working electrode shown in black and traces collected with modified electrodes are color-coded to correspond to the voltammograms in panel **A**. All voltammograms collected in 0.25 M [$NBu_4$][$PF_6$] acetonitrile at 0.1 V $s^{-1}$ using a glassy carbon working electrode.

## SI-4 Additional evidence of EEC reactivity

### *Potential-step experiments*

Chronoamperometry experiments in a solution of 10 mM $[Ni(P^{Ph}_2N^{Ph}_2)_2]^{2+}$ provided further evidence for an EEC reaction pathway in which the formation of the doubly-reduced $[Ni(P^{Ph}_2N^{Ph}_2)]$ is necessary to initiate the follow-up chemical reaction. To deconvolute the role of each redox state, the electrode was stepped to potentials (1) positive of the two redox couples (-0.6 V) where $[Ni(P^{Ph}_2N^{Ph}_2)_2]^{2+}$ will be the dominant species in solution (**Figure S17**, red dashed line), (2) at the cathodic peak potential for the $Ni^{II/I}$ couple (-0.86 V) where $[Ni(P^{Ph}_2N^{Ph}_2)_2]^{+}$ is expected to be the dominant species in solution (**Figure S17**, black dashed line), and (3) at potentials negative of the $Ni^{I/0}$ reduction potential (-1.35 V) where $[Ni(P^{Ph}_2N^{Ph}_2)_2]$ will be the dominant redox state (**Figure S17**, blue dashed line). Chronoamperograms (**Figure S18A**) were then converted to the corresponding Cottrell plot (**Figure S18B**) by plotting current as a function of $t^{-1/2}$. For electrolysis of a homogeneous species under diffusion control, the current will have an inverse $t^{1/2}$ dependence leading to a linear Cottrell plot described by the Cottrell equation (eq. S2)

$$i(t) = \frac{nFAD^{1/2}C^*}{\pi^{1/2}t^{1/2}} \qquad \text{(S2)}$$

where F is the Faraday constant, D is the diffusion coefficient ($cm^2\ s^{-1}$), C* is the concentration of analyte, and A is the electrode surface area ($cm^2$).

While the anticipated *i*-$t^{1/2}$ relationship is observed when the electrode is stepped to potentials where $[Ni(P^{Ph}_2N^{Ph}_2)_2]^{2+}$ and $[Ni(P^{Ph}_2N^{Ph}_2)]^{+}$ are dominant, a sharp decrease in the Cottrell plot is observed when the electrode is stepped to potentials negative of the $Ni^{I/0}$ couple. This negative deviation from linearity is consistent with deposition of an inhibiting material that effectively decreases the electroactive surface area until complete passivation is observed.[2]

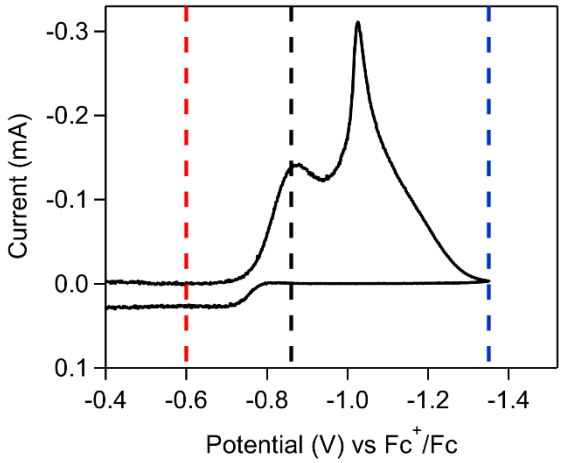


**Figure S17** Cyclic voltammogram of 10 mM $[Ni(P^{Ph}_2N^{Ph}_2)_2]^{2+}$ showing the three step potentials used during chronoamperometry experiments: -0.6 V (red), -0.86 V (black), and -1.35 V (blue). Cyclic voltammogram was recorded at 0.1 V $s^{-1}$ in a solution of 0.25 M $[NBu_4][PF_6]$ acetonitrile using a glassy carbon working electrode.

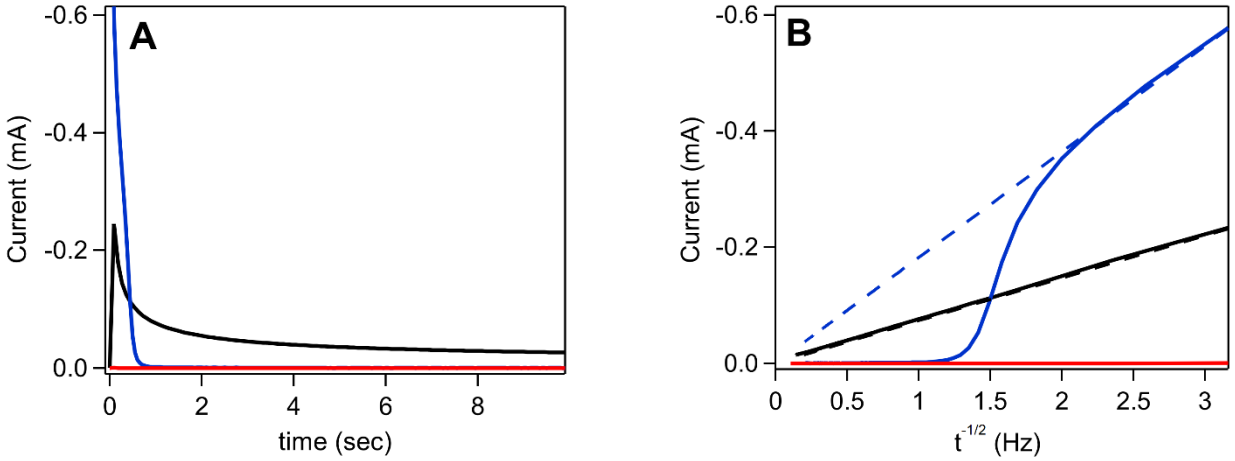


**Figure S18 (A)** Chronoamperograms collected in a solution of 10 mM $[Ni(P^{Ph}_2N^{Ph}_2)_2]^{2+}$ using step potentials of -0.6 V (red), -0.86 V (black), and -1.35 V (blue). **(B)** Corresponding Cottrell plots generated upon converting the x-axis to $t^{-1/2}$ (traces color-coded to match their corresponding chronoamperograms). Experimental data shown as solid lines and dashed lines represent the response predicted by the Cottrell equation for electrolysis of a diffusion-controlled species. Chronoamperograms collected in a solution of 0.25 M $[NBu_4][PF_6]$ acetonitrile using a glassy carbon working electrode.

### *Monitoring Fc wave as a function of induction period potential*

Further support for an EEC reaction mechanism came from induction period experiments which exploited the ferrocene-catalyzed stripping wave as a means of monitoring film formation. In these experiments, the electrode was held at a resting potential and then scanned from this resting potential through the $Fc^{+/0}$ redox couple. The length of this induction period was held constant and the potential was varied. No anodic current enhancement at the $Fc^{+/0}$ redox couple was observed for resting potential values where $[Ni(P^{Ph}_2N^{Ph}_2)_2]^{2+}$ or $[Ni(P^{Ph}_2N^{Ph}_2)_2]^{+}$ are the dominant species in solution. Anodic current enhancement is observed upon reaching potentials where $[Ni(P^{Ph}_2N^{Ph}_2)_2]$ is dominant, consistent with the proposed EEC reaction mechanism.

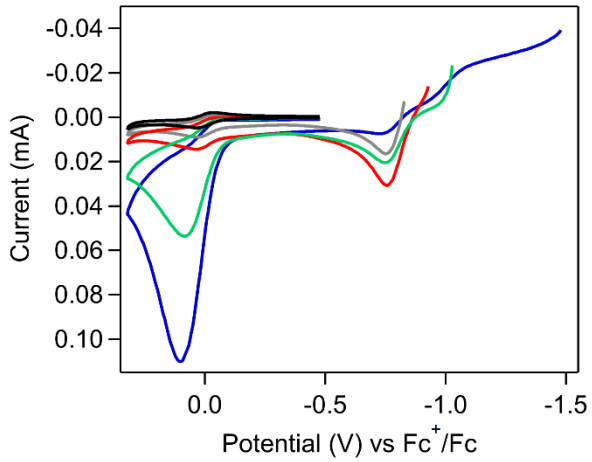


**Figure S19** Cyclic voltammograms of 4.9 mM $[Ni(P^{Ph}_2N^{Ph}_2)_2]^{2+}$ with 0.1 mM ferrocene after 20 second induction periods at -0.48 V (black), -0.83 V (grey), -0.93 V (red), -1.03 V (green), and -1.48 V (blue). Voltammograms obtained at 0.1 V $s^{-1}$ in 0.25 M $[NBu_4][PF_6]$ acetonitrile using a glassy carbon working electrode.

## SI-5 Additional quantification of Fc-catalysed wave

### *Monitoring anodic peak current for Fc redox couple: transition between regime 1 and 2*

As shown in **Figure 6** in the main text, the loss of the anodic peak current for the $Ni^{II/I}$ (**Figure S20**, blue dots) and $Ni^{I/0}$ couple (**Figure S20**, red dots) upon increasing the concentration of $[Ni(P^{Ph}{}_2N^{Ph}{}_2)_2]^{2+}$ from 0.5 mM to 2 mM (concentrations which correspond to regime 1 and 2, respectively) is paralleled by an increase in the anodic peak current at the Fc redox couple (**Figure S20**, black dots) relative to the current predicted by the Randles-Sevcik equation (**Figure S20**, grey dashed line). This is consistent with the role of Fc as a redox mediator which only serves to shuttle electrons between $[Ni(P^{Ph}{}_2N^{Ph}{}_2)_2]$ and the electrode when heterogenization of $[Ni(P^{Ph}{}_2N^{Ph}{}_2)_2]$ results in a loss of electronic communication.

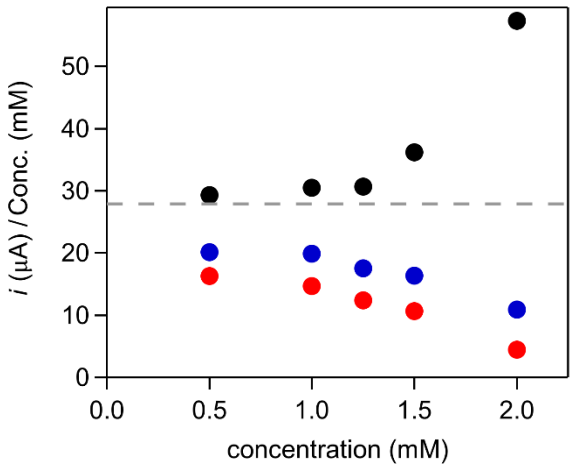


**Figure S20** Quantification of the anodic peak current for the $Ni^{I/0}$ (red dots), $Ni^{II/I}$ (blue dots), and $Fc^{+/0}$ (black dots) redox couple for voltammograms shown in **Figure 6** in the main text. The anodic peak current for the $Fc^{+/0}$ couple predicted by the Randles-Sevcik equation shown as grey dashed line. Ratio of $[Ni(P^{Ph}{}_2N^{Ph}{}_2)_2]^{2+}$:Fc concentration is 1:1.

### *Comparing the rate of $[Ni(P^{Ph}{}_2N^{Ph}{}_2)_2]^{2+}$ regeneration with and without ferrocene*

*UV-vis spectroelectrochemistry*

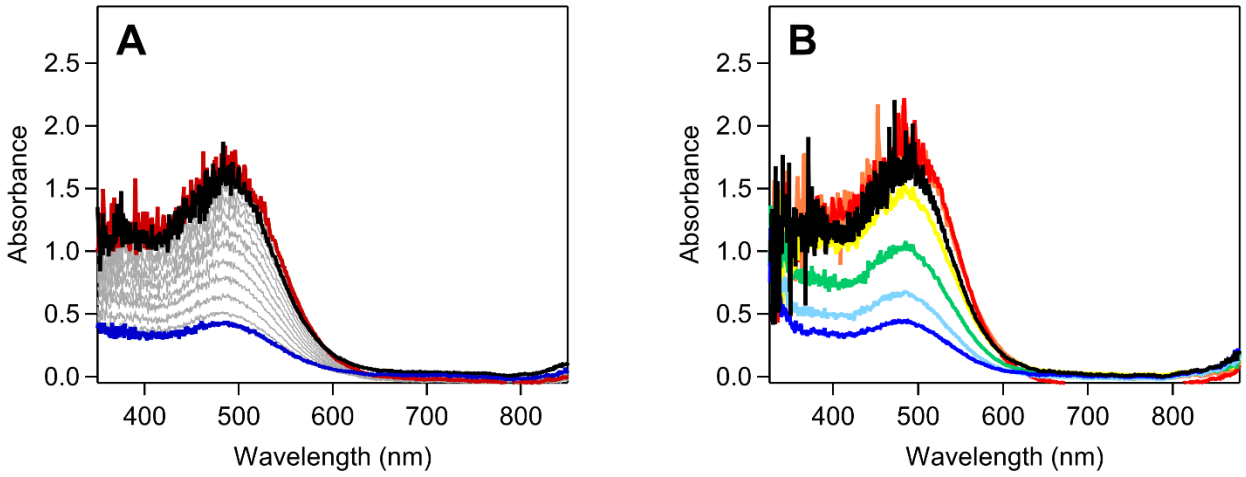


**Figure S21** Select spectra for absorbance data shown in **Figure 7B**. **(A)** UV-vis absorbance measurements collected in a solution of 5 mM $[Ni(P^{Ph}{}_2N^{Ph}{}_2)]^{2+}$ prior to cyclic step chronoamperometry (black), after holding the honeycomb electrode at -1.5 V for 60 seconds (blue), and after stepping the potential to 0.3 V (grey to red). During step 2, spectra were collected every 5 seconds for up to 60 seconds (red). **(B)** UV-vis absorbance measurements collected in a solution of 5 mM $[Ni(P^{Ph}{}_2N^{Ph}{}_2)_2]^{2+}$ with 0.25 mM ferrocene prior to cyclic step chronoamperometry (black), after holding the honeycomb electrode at -1.5 V for 60 seconds (blue), and after stepping the potential to 0.3 V for 5 (light blue), 10 (green), 15 (yellow), 20 (orange), and 25 (red) seconds. All spectroelectrochemistry experiments conducted in 0.25 M $[NBu_4][PF_6]$ acetonitrile with a honeycomb electrode.

*Cyclic Step Chronoamperometry*

To electrochemically evaluate whether the presence of ferrocene accelerates the rate of oxidative delamination, cyclic step chronoamperometry was conducted in solutions of 5, 7.5, and 10 mM $[Ni(P^{Ph}{}_2N^{Ph}{}_2)_2]^{2+}$ in the absence and presence of sub-stochiometric amounts of ferrocene. The electrode was stepped from -0.2 to -1.5 V for 10 or 20 seconds in order to generate heterogeneous $[Ni(P^{Ph}{}_2N^{Ph}{}_2)_2]$ and then stepped to 0.3 V for 30 seconds. In all cases, comparable amounts of current was passed in the forward step with complete current inhibition observed when working at concentrations of 7.5 and 10 mM $[Ni(P^{Ph}{}_2N^{Ph}{}_2)_2]^{2+}$. However, notable deviations were observed when the electrode was stepped to oxidizing potentials. In the presence of ferrocene, a large current spike is observed at early times points followed by a rapid decrease which ultimately converges on the diffusion-controlled current expected for homogeneous ferrocene per the Cottrell equation (eq. S2), behavior consistent with the rapid removal of the inhibiting material. In contrast, only a small increase in current is observed at initial time points in

chronoamperograms collected in the absence of ferrocene followed by a slow current decay, consistent with a far slower rate of oxidation and film delamination.

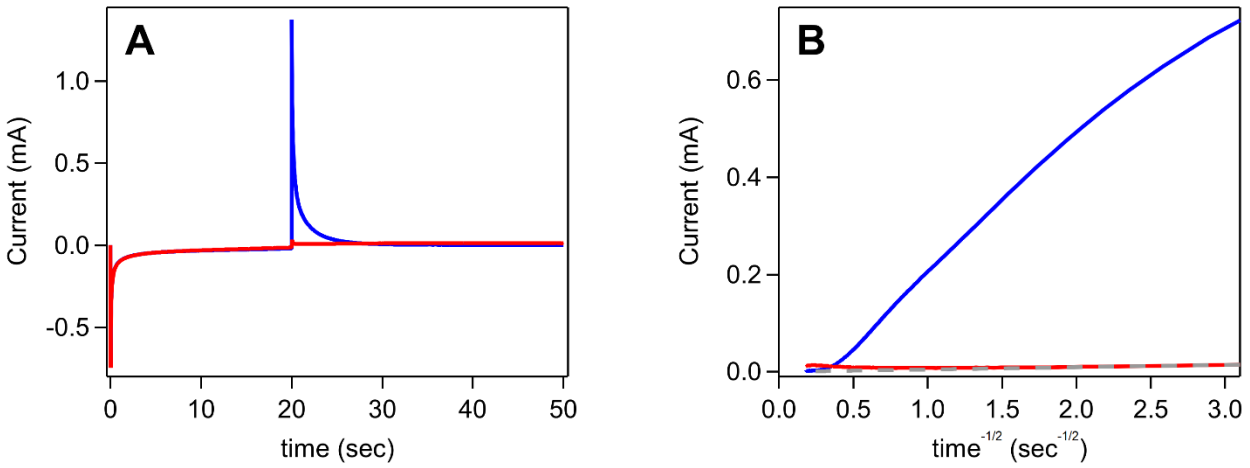


**Figure S22 (A)** Cyclic step chronoamperometry and **(B)** corresponding Cottrell plots recorded in a solution of 5 mM $[Ni(P^{Ph}{}_2N^{Ph}{}_2)_2]^{2+}$ in the absence (red) or presence of 0.25 mM (blue) ferrocene. Dashed grey line in panel **B** represents the linear response predicted by the Cottrell equation for 0.25 mM diffusional ferrocene. All chronoamperograms recorded in 0.25 M $[NBu_4][PF6]$ acetonitrile with a glassy carbon electrode.

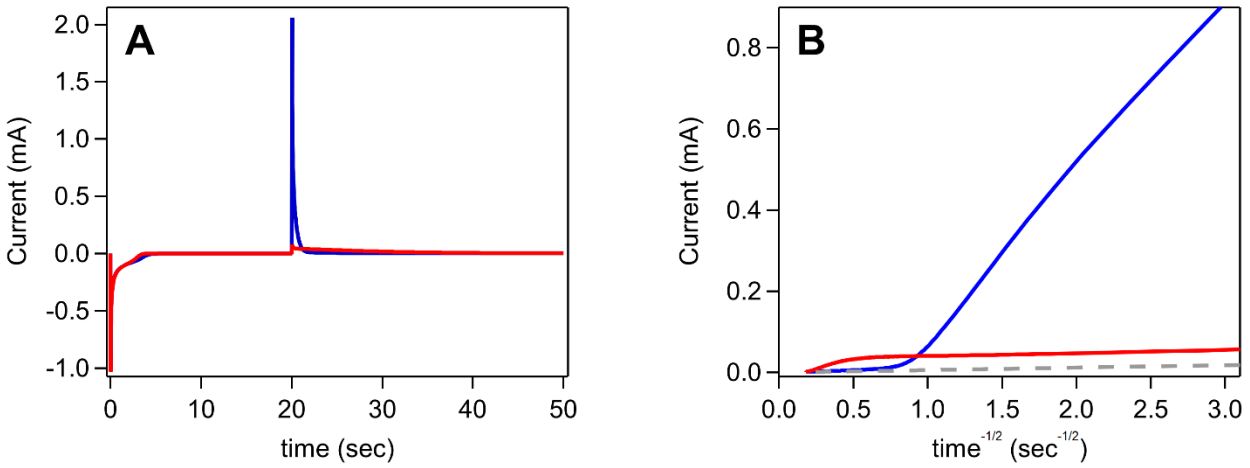


**Figure S23 (A)** Cyclic step chronoamperometry and **(B)** corresponding Cottrell plots recorded in a solution of 7.5 mM $[Ni(P^{Ph}{}_2N^{Ph}{}_2)_2]^{2+}$ in the absence (red) or presence of 0.325 mM (blue) ferrocene. Dashed grey line in panel **B** represents the linear response predicted by the Cottrell equation for 0.325 mM diffusional ferrocene. All chronoamperograms recorded in 0.25 M $[NBu_4][PF6]$ acetonitrile with a glassy carbon electrode.

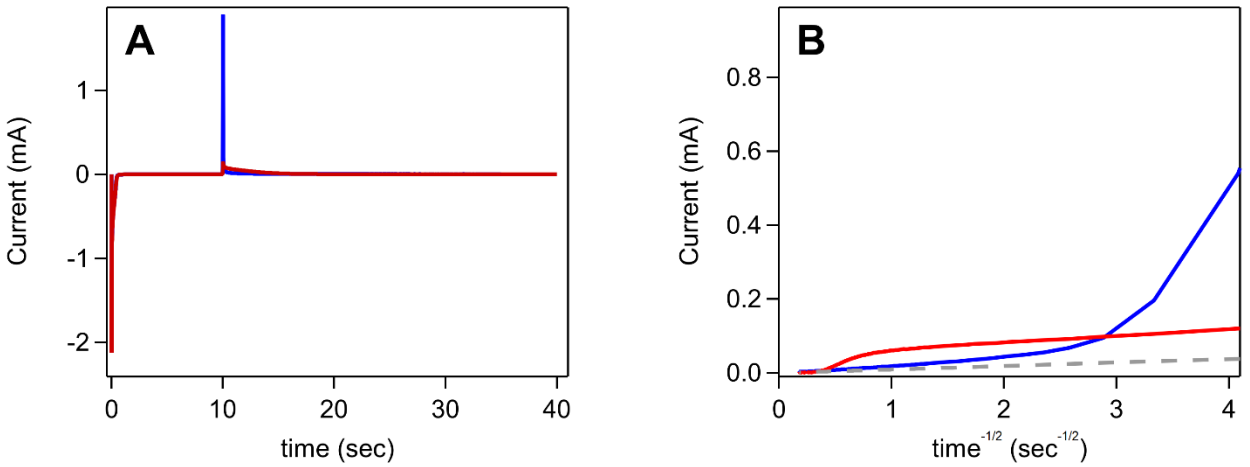


**Figure S24 (A)** Cyclic step chronoamperometry and **(B)** corresponding Cottrell plots recorded in a solution of 10 mM $[Ni(P^{Ph}{}_2N^{Ph}{}_2)_2]^{2+}$ in the absence (red) or presence of 0.5 mM (blue) ferrocene. Dashed grey line in line in panel **B** represents the linear response predicted by the Cottrell equation for 0.5 mM diffusional ferrocene. All chronoamperograms recorded in 0.25 M $[NBu_4][PF6]$ acetonitrile with a glassy carbon electrode.

### *Monitoring the competition between direct oxidation and Fc-catalysed oxidation*

As shown in **Figure 11**, a competition exists between Fc-catalysed oxidation of heterogeneous [Ni($P^{Ph}_2N^{Ph}_2$)$_2$] and direct oxidation at the electrode surface, with the sluggish direct oxidation dominating at slower scan rates and Fc-catalysed oxidation dominating at faster scan rates. This competition can be easily visualized by determining the total charge passed during the broad, direct oxidation wave and the Fc-catalysed wave and then comparing these two values to the total amount of anodic charge passed during the return sweep (starting at potentials positive of -0.8 V). As shown in **Figure S25**, the broad oxidative wave (**Figure S25**, red dots) constitutes nearly 80% of the total anodic charge at the lowest scan rate sampled (0.025 V $s^{-1}$), but the contribution from this broad feature rapidly drops as concentration is increased. This is of course paralleled by an increase in the contribution from Fc-catalysed oxidation (**Figure S25**, blue dots) which plateaus at approximately 90% of the total anodic charge at scan rates of 0.5 V $s^{-1}$ and higher.

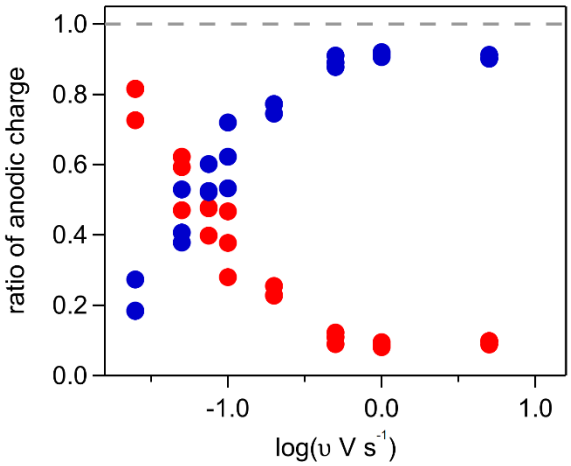


**Figure S25** The competition between direct and Fc-catalysed oxidation (shown in **Figure 11** in the main text) can be visualized by comparing the ratio of the anodic charge passed during the broad oxidative feature (red dots) to the ratio of the anodic charge passed during Fc-catalysed stripping (blue dots) as a function of scan rate. Voltammograms at each scan rate were run in triplicate.

## SI-6 Additional information for induction period studies

### *Determining whether complete passivation is observed during induction periods*

For the induction period studies described in the main text, the length of induction period was used as a handle to control the amount of material deposited ($\Gamma_A^0$) prior to the voltammogram. As the induction period controls the amount of time available for film formation, increasing its length will increase $\Gamma_A^0$ unless the electrode is passivated during this time. If the electrode is passivated during the induction period, no additional [Ni($P^{Ph}_2N^{Ph}_2$)$_2$] can be generated and $\Gamma_A^0$ will reach a maximum value.[4] Two criteria were used to determine whether the electrode was full passivated during the induction period. The first was simply visually inspecting the voltammogram collected after the induction period. These voltammograms started at -1.5 V and the potential was then swept through the $Fc^{+/0}$ couple. If the electrode is completely passivated during the induction period, then the current at the start of the scan will be zero until reaching ca. -0.8 V, at which point direct oxidation of the deposited material would lead to desorption of the material, akin to the behavior observed for the fully passivated electrodes in regime 3 (**Figure 4**).

As the current cannot be measured during an induction period, separate chronoamperometry experiments were also used to evaluate whether complete inhibition could be accomplished during this induction period. Chronoamperometry is a constant potential method in which the electrode is stepped to a potential – akin to the hold time used during the induction period experiments – and the current is recorded as a function of time.[2] Induction period experiments presented in the main text used $[Ni(P^{Ph}_2N^{Ph}_2)_2]^{2+}$ concentrations of 3 mM (**Figure 8**) or 5 mM (**Figure 9** and **Figure 10**) and used hold times of either 1-20 seconds or 5-10 seconds, respectively. To probe whether inhibition can occur during this timeframe, chronoamperometry experiments were conducted in solution of 3 and 5 mM $[Ni(P^{Ph}_2N^{Ph}_2)_2]^{2+}$ where the working electrode was stepped to -1.35 V and held at this potential for 20 seconds. Converting these chronoamperograms to their corresponding Cottrell plot and comparing these plots to the diffusion-controlled current predicted by the Cottrell equation (equation S2) shows that complete inhibition does not occur within 20 seconds at either concentration (**Figure S26**).

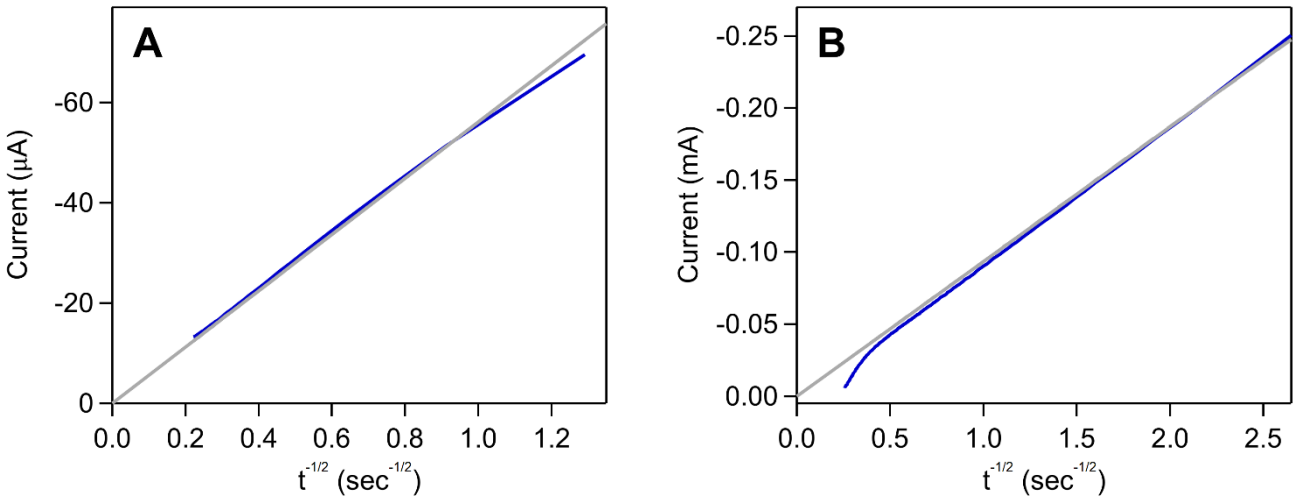


**Figure S26** Cottrell plots for chronoamperometry experiments conducted in **(A)** 3 mM and **(B)** 5 mM $[Ni(P^{Ph}{}_2N^{Ph}{}_2)_2]^{2+}$ to evaluate whether electrode passivation occurs within 20 seconds. Experimental data shown in blue and the diffusion-controlled current predicted by the Cottrell equation shown in grey. Chronoamperograms recorded in 0.25 M $[NBu_4][PF_6]$ acetonitrile using a glassy carbon working electrode.

### *Monitoring the loss of the ferrocene cathodic peak during ferrocene titrations*

The magnitude of the return feature for a catalyst redox couple is expected to decrease as the degree of substrate consumption decreases, where the degree of substrate consumption will be inversely related to the substrate-to-catalyst ratio defined by the excess factor $\gamma = \Gamma_A^0/C_P^0$. The degree of substrate consumption can thus be decreased by decreasing the concentration of catalyst $C_P^0$ (in this case ferrocene) constant while keeping the amount adsorbed substrate $\Gamma_A^0$ (in this case adsorbed $[Ni(P^{Ph}{}_2N^{Ph}{}_2)_2]$) constant.[5] The impact of catalyst concentration at a constant $\Gamma_A^0$ was established via induction period studies which varied the concentration of ferrocene (0.1 – 0.6 mM) at a constant induction period (5 seconds). To quantify this for the ferrocene titrations shown in (**Figure 9A**), the ratio of the experimentally observed cathodic current for the $Fc^{+/0}$ redox couple $i_{p,c}(Fc^{+/0})$ to the theoretical value of the $Fc^{+/0}$ redox couple predicted by the Randles-Sevcik equation $i_{p,c}^{o}(Fc^{+/0})$ was monitored as a function of ferrocene concentration. At the lowest ferrocene concentration employed (0.1 mM), $i_{p,c}(Fc^{+/0})$ was far smaller than $i_{p,c}^{o}(Fc^{+/0})$ and the ratio of the experimental to theoretical peak current ($i_{p,c}(Fc^{+/0})/i_{p,c}^{o}(Fc^{+/0})$) increased as a function of ferrocene concentration, from 0.08 at 0.1 mM to 0.36 at 0.6 mM (**Figure S27**).

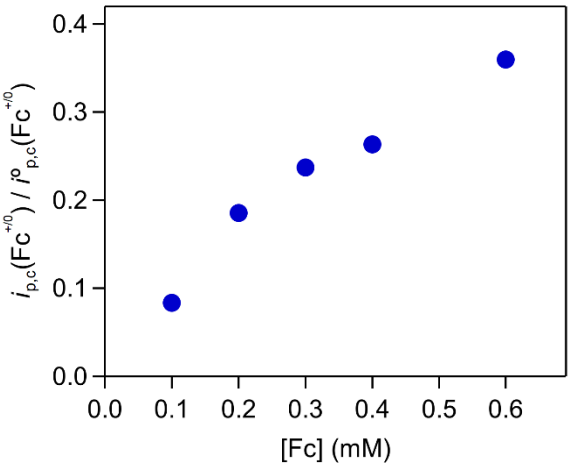


**Figure S27** The ratio of the experimental to theoretical cathodic peak current for the $Fc^{+/0}$ redox couple ($i_{p,c}(Fc^{+/0})/i_{p,c}^{o}(Fc^{+/0})$) increased as a function of ferrocene concentration during induction period studies conducted in 5 mM $[Ni(P^{Ph}{}_2N^{Ph}{}_2)_2]^{2+}$ using a glassy carbon working electrode and a 5 second induction period (**Figure 9A**), as expected for a catalytic wave.

Alternatively, the degree of substrate consumption can be decreased by increasing $\Gamma_A^0$ while keeping $C_P^0$ constant. To evaluate the impact of $\Gamma_A^0$ at a constant ferrocene concentration, induction period studies were conducted which varied the length of the induction period from 0 to 20 seconds (**Figure 8**). These trials show a subtle decrease in the magnitude of $i_{p,c}(Fc^{+/0})$ with increasing induction period length (**Figure S28**), as expected for an EC′ mechanism.

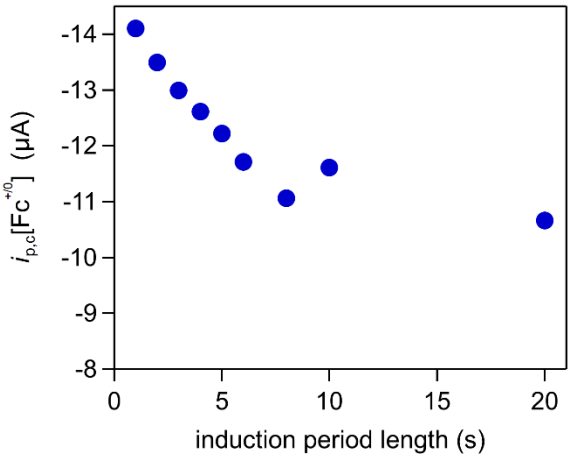


**Figure S28** Because the induction period length can be used as a proxy for the magnitude of $\Gamma_A^0$, monitoring the cathodic peak current for the ferrocene redox couple as a function of induction period length gives insight into the influence of $\Gamma_A^0$ on the degree of substrate consumption. The subtle decrease in $i_{p,c}[Fc^{+/0}]$ with increasing induction period length is consistent with a scheme in which more $Fc^+$ is reduced via catalytic turnover as the amount of adsorbed substrate increases.

### *Relationship between scan rate and $\Gamma_A^0$ during induction period length studies*

For a catalytic system involving a homogeneous catalyst and homogeneous substrate, the degree of substrate consumption will decrease as scan rate increases because there is less time available during the potential sweep to consume substrate consumption. Holding $\gamma$ constant while increasing $\upsilon$ will thus result in a decrease in the magnitude of return feature for the catalytic wave followed by a transition in the shape of the catalytic wave from a peak to a steady-state plateau. However, when evaluating the relationship between $\upsilon$ and the degree of substrate consumption for a catalytic system involving a heterogeneous substate and homogeneous catalyst using the induction period studies described in the main text, when working at very low scan rates, this relationship is more complex when working at very slow scan rates because $\upsilon$ will also influence $\Gamma_A^0$ and, by extension, $\gamma$ (another variable which controls the degree of substrate consumption). There are two specific ways that $\upsilon$ will influence $\Gamma_A^0$ in this system:

**(1)** The magnitude of $\Gamma_A^0$ deposited during the cyclic voltammogram at reducing potentials will increase at slower scan rates.

During induction period studies, material will be deposited whenever the electrode is held at potentials that are sufficiently negative to generate additional [Ni($P^{Ph}_2N^{Ph}_2$)$_2$]. As is discussed in the main text, material will be deposited during the induction period when the electrode is held at -1.5 V. However, during the subsequent potential sweep, the electrode is scanned from the potential held during the induction period through the $Fc^{+/0}$ redox couple. As such, there is an initial potential range during the cyclic voltammogram (-1.5 V to ca. -0.8 V) in which additional material deposits. If a constant scan rate is used, then the amount of material deposited during that portion of the potential sweep will be constant and thus will not convolute analysis. However, when scan rate is increased, the amount time spent in that potential range decreases thereby decreasing the amount of additional material deposited.

**(2)** The magnitude of $\Gamma_A^0$ removed via direct oxidation at oxidizing potential will increase at slower scan rates

As shown in **Figure 11**, there is a direct competition between electrochemical and Fc-mediated oxidation. This is because direct oxidation starts at more positive potentials (ca. -0.8 V) such that additional material can be removed in the potential window between ca. -0.8 V and the Fc redox couple ($E_{1/2}$ = 0 V). The amount that this direct oxidation influences $\Gamma_A^0$ will depend on the amount of time spent in this potential range, which is again dictated by the scan rate. For this system in particular, the kinetics of this direct oxidation are so slow, that this process is uncompetitive when working at faster scan rates as shown in

**Figure 4**. At sufficiently fast scan rates, direct oxidation can be considered negligible and catalytic oxidation can be approximated as the only operative pathway.

As both of these processes will become increasingly uncompetitive as scan rate is increased, the influence of scan rate on $\Gamma_A^0$ will be negligible above a certain scan rate threshold. As such, at these sufficiently large scan rates, the more simple relationship between scan rate and the degree of substrate consumption that has been established for purely homogeneous catalytic systems will be observed for the adsorbed substrate-homogeneous catalyst system described in the main text, as shown in **Figure 10**.

## References


(1) Elgrishi, N.; Rountree, K. J.; McCarthy, B. D.; Rountree, E. S.; Eisenhart, T. T.; Dempsey, J. L. A Practical Beginner's Guide to Cyclic Voltammetry. *J. Chem. Educ.* **2018**, *95* (2), 197–206. https://doi.org/10.1021/acs.jchemed.7b00361.

(2) Bard, A. J.; Faulkner, L. R. *Electrochemical Methods: Fundamentals and Applications*, 2nd ed.; Harris, D., Swain, E., Robey, C., Aiello, E., Eds.; John Wiley & Sons, Inc.: Hoboken, NJ, USA, 2001.

(3) Kaeffer, N.; Morozan, A.; Fize, J.; Martinez, E.; Guetaz, L.; Artero, V. The Dark Side of Molecular Catalysis: Diimine–Dioxime Cobalt Complexes Are Not the Actual Hydrogen Evolution Electrocatalyst in Acidic Aqueous Solutions. *ACS Catal.* **2016**, *6* (6), 3727–3737. https://doi.org/10.1021/acscatal.6b00378.

(4) Downard, A. J. Potential-Dependence of Self-Limited Films Formed by Reduction of Aryldiazonium Salts at Glassy Carbon Electrodes. *Langmuir* **2000**, *16* (24), 9680–9682. https://doi.org/10.1021/la000866i.

(5) Savéant, J.-M. *Elements of Molecular and Biomolecular Electrochemistry*; John Wiley & Sons, Inc.: Hoboken, NJ, USA, 2006.